"On the Use of Microwave Radiometers for Deep Space Mission Applications by Means of a Radiometric-Based Scalar Indicator"

Bosisio, Ada Vittoria ; Graziani, Alberto ; Mattioli, Vinia ; Tortora, Paolo

Abstract

The estimation of the path delay due to water vapor is a crucial aspect for the calibration of the Doppler observables of a deep space probe. The advanced water vapor radiometer (AWVR) developed by the Jet Propulsion Laboratory (JPL, NASA) already proved its capability to accurately estimate the path delay during the entire Cassini mission. Here, from the AWVR measurements, a scalar sky status indicator (SSI) was developed as a criterion for selecting the radiometric path delay estimations in the orbit determination process. Results indicate that the use of such index allows a reduction of the range rate residual root mean square (rms).

Document type : *Article de périodique (Journal article)*

Référence bibliographique

Bosisio, Ada Vittoria ; Graziani, Alberto ; Mattioli, Vinia ; Tortora, Paolo. *On the Use of Microwave Radiometers for Deep Space Mission Applications by Means of a Radiometric-Based Scalar Indicator.* In: *IEEE Journal of Selected Topics in Applied Earth Observations and Remote Sensing*, Vol. PP, no.99, pp. 1-9 (June 2015)

DOI : 10.1109/JSTARS.2015.2443174

On the Use of Microwave Radiometers for Deep Space Mission Applications by Means of a Radiometric-Based Scalar Indicator

Ada Vittoria Bosisio, *Member, IEEE*, Alberto Graziani, Vinia Mattioli, and Paolo Tortora, *Member, IEEE*

***Abstract*—The estimation of the path delay due to water vapor is a crucial aspect for the calibration of the Doppler observables of a deep space probe. The advanced water vapor radiometer (AWVR) developed by the Jet Propulsion Laboratory (JPL, NASA) already proved its capability to accurately estimate the path delay during the entire Cassini mission. Here, from the AWVR measurements, a scalar sky status indicator (*SSI*) was developed as a criterion for selecting the radiometric path delay estimations in the orbit determination process. Results indicate that the use of such index allows a reduction of the range rate residual root mean square (rms).**

***Index Terms*—Microwave radiometers, tropospheric path delay, orbit determination.**

I. Introduction

MANY WORKS demonstrate the advantages of employing ground-based microwave radiometers (MWRs) over a variety of environmental and engineering applications, including meteorological observations and forecasting [1]–[3], communications [4], [5], geodesy and long-baseline interferometry [6], satellite validation [7], climate [8], fundamental molecular physics [9], and deep space radioscience experiments [10]. Reasons for the utility of MWRs measurements, in particular at 23.8 and 31.4 GHz, are their sensitivity to the atmospheric water vapor and cloud liquid, and their reliability for the accurate estimation of the integrated quantities of those parameters, namely, the integrated precipitable water vapor (IWV) and the integrated cloud liquid water content (LWC). Specifically, accuracy is about 0.4 mm for IWV and 0.02 mm for LWC [11], [12]. An additional important feature of MWRs is the nearly continuous observational capability on time scales of seconds to minutes.

In the framework of deep space probe navigation and radio science experiments, the assessment of the tropospheric path delay plays a crucial role since it is one of the main error sources of the deep-space observables [13]. Among the different techniques available to estimate the tropospheric path delay, the use of MWRs is the most accurate one to estimate the component due to water vapor [14]. The Solar Conjunction Experiment 1 (SCE1) [10], carried out during the cruise phase of the NASA/ESA/ASI Cassini mission to Saturn, demonstrated the importance of an accurate estimation of the tropospheric path delay, particularly, if the solar plasma noise is removed with the so-called multifrequency link [15].

To account for the tropospheric path delay, NASA's deep space network (DSN) complexes are equipped with the so-called tracking system analytic calibration (TSAC). As detailed in [16], TSAC is the standard automated troposphere calibration system developed at Jet Propulsion Laboratory (JPL) for deep space probe navigation purposes, which relies on the zenith path delay estimates derived from global positioning system (GPS) observations.

To support Cassini's cruise radio science experiments, a new generation of media calibration systems was developed by JPL, the advanced media calibration (AMC) system consisting of an advanced water vapor radiometer (AWVR), a surface meteorological (SM) station and a microwave temperature profiler (MTP) [17]. Two AMC units were developed; one is installed at the Goldstone DSN complex, USA, close to the DSS 25 (Deep Space Station), and the other is at the Robledo DSN complex, Spain, close to the DSS 55. The accuracy of the TSAC calibrations to estimate up to 90% of the zenith path delay is sufficient to solve the orbit determination (OD) problem [13] for probe navigation purposes. On the other hand, a higher precision solution of the OD problem is required for scientific purposes. In this case, although the TSAC calibration could be applied, the AMC calibration may be the preferred choice, according to its availability at the DSN site. Indeed, AMC gives intrinsically more precise slant wet path delay (SPD) estimation along the line-of-sight (LOS), notwithstanding its use is still limited in radio science experiments due to the poor performance in cloudy/rainy scenarios compared to the GPS-based estimation.

The present study aims at addressing the use of the AMC approach with respect to the TSAC through the implementation of an atmospheric index, a scalar quantity named sky status indicator (*SSI*) [18], based on the radiometer measurements. The *SSI* capability of validating the use of AMC retrieved path delay in the calibration of the deep space navigation observables is addressed by analyzing the quality of Cassini's range

Manuscript received August 31, 2014; revised April 21, 2015; accepted May 26, 2015.

A. V. Bosisio is with the Institute of Electronics, Computer and Telecommunication Engineering, National Research Council of Italy, Milano I-20133, Italy (e-mail: adavittoria.bosisio@ieiit.cnr.it).

A. Graziani is with ICTEAM, Department of Electronic Engineering, Université Catholique de Louvain, Louvain-la-Neuve B-1348, Belgium (e-mail: alberto.graziani@uclouvain.be).

V. Mattioli is with HE Space Operations GmbH, Darmstadt D-64295, Germany (e-mail: vinia.mattioli@eumetsat.int).

P. Tortora is with the Department of Industrial Engineering, University of Bologna, Bologna I-40136, Italy (e-mail: paolo.tortora@unibo.it).

Color versions of one or more of the figures in this paper are available online at http://ieeexplore.ieee.org.

Digital Object Identifier 10.1109/JSTARS.2015.2443174

rate residuals obtained using different troposphere calibration datasets. The probe velocity with respect to the Earth (the so-called range rate) was reconstructed by means of precise measurements of the Doppler shift of a highly stable microwave radio link between Cassini and the ground station antennas of NASA's DSN. The root mean square (rms) of the AMC-based range rate residuals was computed and compared to the one obtained through the standard TSAC procedure. A reduction of rms of the residuals gives a clear indication that the advanced calibration process is more effective than the standard one in estimating the tropospheric path delay.

This paper is organized as follows. In Section II, an overview of the process of the Cassini gravitational flybys and its dataset for the study is given. In Section III, the *SSI* algorithm development and the methodology of its application are explained. In Section IV, results of the analysis on the range rate observable residuals are presented. Finally, in Section V, conclusion is discussed.

II. Cassini Gravitational Flybys Dataset

The comparison of AMC and TSAC approaches relies on the range rate residuals of the OD solution computed on a set of gravitational flybys of Saturn and some of its icy moons acquired during the tour phase of the Cassini mission to estimate the gravity field of the target body [19], [20]. The following sections briefly describe the main systems and dataset used in our study.

A. Selected Cassini's Flybys and OD Process

For the typical geometry of the flybys, the tracking of Cassini may require up to two or three consecutive Earth days. In this time, the three NASA DSN complexes track the spacecraft and the stations involved may collect more than one pass per flyby. In our study, we used the flybys collected at the DSS 25 antenna at Goldstone. Table I reports the list of the 10 selected flybys with the date of the event and the number of passes available for each flyby. For all the selected cases, our data set is represented by TSAC time series (Section II-B), the AMC time series (Section II-C) and the two OD solutions obtained calibrating the Cassini observables with the two mentioned techniques.

As far as the OD solutions are concerned, these are computed with the NASA JPL Orbit Determination Program (ODP) [21], [22]. For clarity, a brief description of ODP process is reported here. The software computes the least square difference between the deep-space observables, received from the spacecraft and properly weighted by a scalar factor, and the observables computed by a detailed mathematical model. In this process, the troposphere calibration enters as one of the errors affecting the computed observables. The effect of the calibration is visible in the residuals of the least square filtering.

B. TSAC Measurements

TSAC is the tropospheric path delay calibration system developed by JPL to support the tracking and navigation activities of the interplanetary spacecraft [16]. It represents the most reliable and low-cost system capable to provide continuous zenith troposphere calibration for interplanetary spacecraft. According to the current tracking profile, appropriate mapping functions are used to map the zenith path delay along the spacecraft LOS. TSAC calibration is obtained by processing with the JPL GIPSY-OASIS II software [23] the GPS observables collected with a geodetic dual-frequency GPS receiver installed at each DSN complex.

TABLE I
List of 10 Selected Gravitational Flybys

Name	Flyby date	Number of passes
Enceladus_E12	30 November 2010	1
Iapetus	10 September 2010	1
Rhea_4	9 March 2013	3
Saturn_Rev28	09 September 2006	1
Saturn_Rev68	17 May 2008	1
Titan_T11	27 February 2006	3
Titan_T22	28 December 2006	2
Titan_T33	29 June 2007	3
Titan_T45	31 July 2008	1
Titan_T68	20 May 2010	1

The TSAC zenith tropospheric delay is then divided into its wet and hydrostatic components, by using surface barometric pressure measurements. Additionally, zenith wet and hydrostatic path delay time series are fitted by polynomials to facilitate interpolation in time. Zenith path delay polynomials are specific for each complex and typically have a time span of 6 h. In our work, the most accurate TSAC zenith path delay estimations are used for the calibration of the analyzed Cassini flybys.

C. AMC Measurements

In the AMC unit, the AWVR represents the core of the system: it is an ultra-stable MWR with steerable antenna capable to point to the spacecraft position in the sky. The AWVR is a three-channel radiometer with observing channels at 22.2, 23.8, and 31.4 GHz, with 600 MHz of bandwidth per channel, and a long-term stability of 10 mK on time scale of 10 000 s. It has an off-axis antenna with a beam width of 1° and very low side lobes. A detailed description of the instrument is given in [17]. Two retrieval algorithms [24], [25] estimate the tropospheric path delay combining the measurements of the AWVR, MTP, and SM.

The operation of the AMC unit is enabled via scripts and pointing predictions for the AWVR. The use of quality flags is available together with the retrieved path delay to represent both the status of the instrument and the retrieved parameters. The computed flags are: ZPD for the zenith path delay retrieval, WND for the wind, SUR for the SM, MTP for the MTP, WVR for the AWVR, and CLD for the presence of clouds which is based on the retrieval of the liquid water LWC. For all the flags, a zero value means that the parameter is in the expected range or that the instrument is correctly working. On the other hand, a different value (typically 1) indicates that parameters are out of the proper range or instruments malfunctioning. CLD flag is 0 if the LWC is below 20 μm, 1 if the LWC is between 20 and

100 μm, 2 if the LWC is between 100 and 200 μm and 3 if the LWC is greater than 200 μm. Hereinafter, these will be referred to as the AMC products.

III. Methodology

In this section, we describe the methodology for the *SSI* computation and its application. *SSI* is defined as the ratio between the brightness temperatures observed at 23.8 and 31.4 GHz, and it is employed to discriminate among LOS sky conditions (clear sky, cloudy, or rainy) to select the most reliable path delay retrievals in the tropospheric correction algorithm. The discriminating aspects of performance within *SSI* were tested in previous works [18], [26] with radiometric observations mainly at zenith or at fixed elevation angles [27]. Here, the method has been further developed for its application to deep-space probes radio tracking, with *SSI* being parameterized as a function of the elevation angle to be commanded by a radiometer equipped with a steering mechanism.

The procedure that we followed for *SSI* implementation needs ancillary information from radiosonde observations (RAOBs), which are described in Section III-A. The *SSI* implementation and the validation of the methodology are described in Section III-B, and *SSI* development is given in Section III-C.

A. RAOBs

RAOBs have been used in this study to parameterize *SSI* as a function of the elevation angle, as described in Section III-B. RAOBs were acquired at the closest RAOB station to Goldstone (WMO 72381, at Edwards CA/AFB), from 1994 to 2014, and are available from the NOAA/Earth System Research Laboratory (ERSL) Global Systems Division archive [28]. RAOB profiles have been additionally quality controlled to keep only the highest quality profiles. The quality-control process is described in [29].

A large database of simulated radiometric brightness temperature observations ($T_B s$) at the AWVR frequency channels was generated at elevation angles from 15° to 90° with 5° interval, by using a radiative transfer algorithm [30]. The model proposed by Rosenkranz [31], [32] for gaseous absorption has been used in applying the radiative transfer scheme and the cloud model in [33] was used to generate cloud liquid water profiles. The resulting database contains 6469 profiles and it spans the entire range of the expected path delay, water vapor, and cloud liquid water conditions.

B. Methodology Description

The procedure is summarized as follows: 1) *SSI* values are computed from simulated radiometric brightness temperatures and the elevation-dependent *SSI* threshold (reference value) between clear and cloudy sky conditions is determined; 2) *SSI* values computed from AWVR measurements acquired during the deep space tracking phase are compared with the proper reference value to discriminate the clear-sky measurements and to trigger the use of the AMC calibration; 3) the OD solution is computed considering the two possible troposphere calibration techniques (TSAC and AMC); and 4) the range rate residuals are compared among the two cases and the indications issued from both the *SSI* screening and the AMC products.

A crucial aspect in our work is the application of the *SSI* index to evaluate the advantage of using the AMC calibration when the instantaneous *SSI* is below the *SSI* threshold. We base our analysis on the comparison of the orbital solution of the selected flybys in terms of range rate residuals (mm/s) obtained by the Cassini Doppler observables. The use of the range rate residuals rather than the Doppler ones is preferred because the Cassini radio science communication link operates in both X-band and Ka-band. In order to process both the collected observables, the two Doppler values are scaled by their corresponding factors to the range rate: the frequency independent term, which maintains all the information available in the Doppler observables. Then, we compare the range rate residuals rms when the observables are calibrated with TSAC and when they are calibrated with AMC. A reduction of the rms residual value indicates a more accurate calibration. For the comparison, we assume that the setup used for the OD solution differs only by the use of the tropospheric calibration.

C. SSI Development

The *SSI* definition and computation are fully described in [18]. Here, for an overview of the approach, the major features are discussed. The basic assumption is that in clear-sky conditions, i.e., when the contribution to the thermal noise is mainly due to the water vapor (besides the small effect of dry gases), the ratio between ground-based brightness temperature measurements collected around 20–30 GHz, respectively, for this radiometer at 31.4 and 23.8 GHz, almost show a linear relationship. As the amount of water content increases or a liquid phase appears, this linear relationship does not hold and the two line frequencies accord a different weight to the water vapor and the cloud liquid along the path. Hence, the ratio $T_B(f_2, \theta)/T_B(f_1, \theta)$ of concurrent radiometric measurements depends on the thermodynamic state of the atmosphere. *SSI* definition is given in (1) [18] by

$$SSI(\theta) = \frac{T_B(31.4, \theta) - c_0(\theta)}{T_B(23.8, \theta)} \tag{1}$$

where $T_B(23.8, \theta)$ and $T_B(31.4, \theta)$ are the brightness temperatures, in K, at frequency channel $f_1 = 23.8\,\text{GHz}$ and $f_2 = 31.4\,\text{GHz}$ measured at elevation angle θ.

For the Goldstone site, the zenithal *SSI* values range from 0.28 up to above 1, depending on the atmospheric conditions. In clear-sky conditions, although *SSI* is not constant, it changes slowly with the water vapor content and a threshold value ($= 0.3$ in our work) is easily identified. As the atmospheric conditions change and some liquid clouds are in the observation path, *SSI* values rapidly increase due to the fact that the channel centered at 31.4 GHz is more sensitive to liquid water than the channel centered at 23.8 GHz. Under rainy conditions, both channels are near the saturation and their ratio, *SSI*, is close to 1 or above.

The computation of *SSI* requires the knowledge of the coefficient c_0, which can be calculated by using either simulated or measured $T_B(f, \theta)$ [26] as the intercept of the best fit performed on couples of $[T_B(23.8), T_B(31.4)]$ strictly referred to clear-sky conditions. From a radiative point of view, c_0 accounts for the atmospheric dry contribution along the observed path. In this study, the parameterizations of both the coefficient $c_0(\theta)$ and the clear-sky $SSI(\theta)$ as a function of elevation angle are addressed, to extend the application of *SSI* to tracking radiometers. As AWVR and DSS antenna track the Cassini spacecraft, measurements are taken at several different observation angles ($6° < \theta < 78°$), and *SSI* values need to be computed accordingly from $T_Bs(f, \theta)$ and angle-dependent $c_0(\theta)$. The objective is to develop theoretical reference values for $c_0(\theta)$ and $SSI(\theta)$ and to use these values as a threshold for actual *SSI* computations from the AWVR radiometer. Then, an actual *SSI* value below the threshold identifies clear-sky conditions along the observation path and triggers the use of AMC path delay retrieval in the OD. The parameterization of both $c_0(\theta)$ and $SSI(\theta)$ expressions was derived from a statistical analysis performed on the simulated brightness temperature dataset described in Section III-A. The dependency on the elevation angle has been expressed in terms of the air mass (AM) coefficient $AM = 1/\sin(\theta)$, with the refinements given in [34] to account for the Earth curvature at low elevation angles

$$AM' = AM - h \cdot AM\left(AM^2 - 1\right)/R_e \qquad (2)$$

where $R_e = 6370.95$ km and $h = 1.9$ km, the Earth radius and an equivalent height value, respectively.

The relationship between the pairs of simulated T_Bs at 23.8 and 31.4 GHz under the hypothesis of clear-sky conditions can be modeled through a linear relationship with fairly good agreement in the elevation angular span comprised between 25° and 90°. At low elevation angles, a nonlinear behavior (quadratic) appears on top of the linear one for high water vapor values as elevation diminishes and, correspondingly, the sensitivity of the brightness temperature to water vapor diminishes. In terms of c_0, as it accounts for the dry contribution of the atmosphere, it was modeled as the intercept of the linear fit of the lower range of T_B's, i.e., the driest conditions.

The computed c_0 values are reported w.r.t. the AM in Fig. 1 (black circles) together with the quadratic fit (red line) that issues from a regression analysis over 1812 couples of brightness temperature values simulated under the driest sky conditions, i.e., $\max\left(T_B\text{s}(23.8, 5°)\right) < 120$ K. The expression of the quadratic fit is as follows:

$$c_0(AM) = -0.08287 \cdot AM^2 + 4.7879 \cdot AM + 2.0258 \quad (3)$$

that models the computed values with a l_1-norm residual $R = \sum_1^{1812} |\widehat{c_0} - c_0| = 0.0175$. Then, the *SSI* values were computed for all 5669 clear-sky RAOBs profiles according to (1). Fig. 2 reports the *SSI* values (gray dots) w.r.t. AM together with the corresponding standard deviation (SD) values (black bars) that span from 0.013 to 0.025 at 90° and 5°, respectively. Though the *SSI* values were computed from clear-sky brightness temperature values, the dispersion about an average value, at each specific elevation angle, accounts for the diverse atmospheric conditions. As expected, the greater the AM value the higher the SD is.

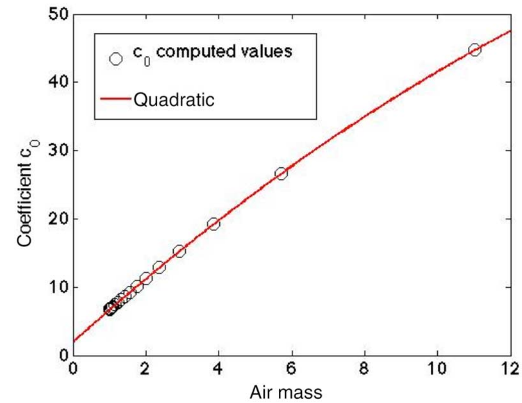

Fig. 1. Quadratic behavior of coefficient c_0 (red line) is derived from the regression fit over the driest 1812 c_0 values (black circles) computed from simulated brightness temperatures RAOBs based.

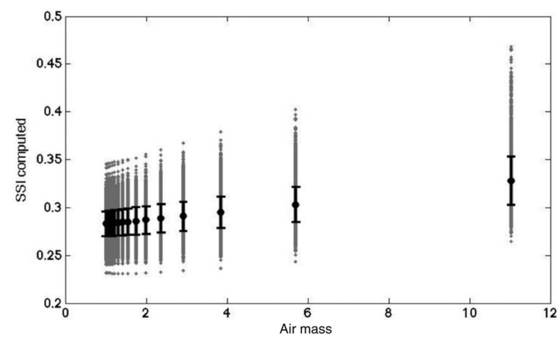

Fig. 2. SSI values (gray dots) with the associated SD values (black bars) with respect to the median value (black dots) versus AM. The *SSI* values are strictly associated to the clear-sky conditions as derived from the RAOBs dataset.

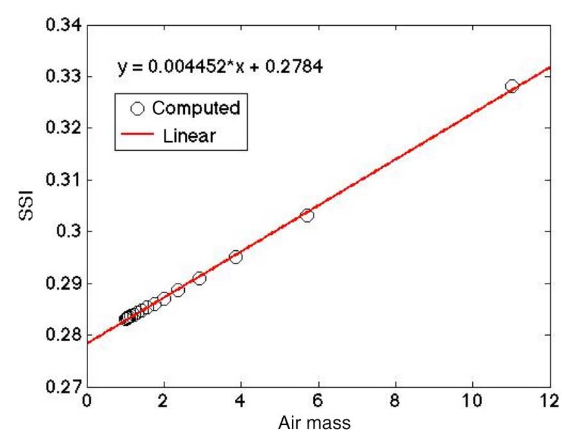

Fig. 3. Average clear-sky *SSI* values (black circles) w.r.t. the AM. The red line represents the linear regression best fit.

As shown in Fig. 3, the regression analysis performed on the average values evidenced the linear relationship between the *SSI* values and the AM ones

$$SSI_{clear\ sky}(AM) = 0.00445 \cdot AM + 0.2784 \qquad (4)$$

that models the computed values with an l_1-norm residual $R = \sum_1^{5669} \left|S\hat{SI} - SSI\right| = 0.0013$.

SSI can be computed similarly by using radiometric measurement alone, provided that the instrument is routinely calibrated

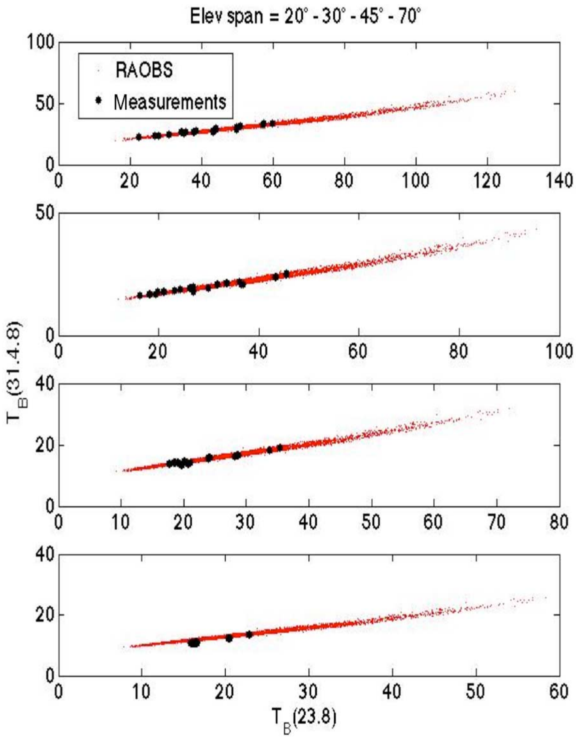

Fig. 4. Scatter diagram of $T_B(31.4)$ versus $T_B(23.8)$ simulated values from RAOBs dataset (red dots) and measured one (black dots) at 20°, 30°, 45°, and 70° from top to bottom.

and that the amount and quality of data are statistically representative of the atmospheric conditions of the measurement site. In our study, the chosen approach for the computation of the coefficient c_0 and of the reference clear-sky *SSI* value has been by using simulations from RAOBs. The choice was mainly driven by the availability of a large dataset of RAOBs, spanning a wide range of path delay, water vapor, and cloud liquid water conditions, compared to a much lesser availability of radiometric measurements to be able to perform a meaningful best fit, especially at different low elevation angles. Also, using a nonlinear correction term for c_0 or *SSI* may be envisaged at lower elevations (below 15°) for specific tracking activities and applications. Measurements and simulations are in good agreement as shown in Fig. 4 where four elevation angles, namely, 20°, 30°, 45°, and 70°, were chosen to compare the two datasets. Due to the different dynamic range of the values represented in the four panels, they were plotted with reference to each specific scale interval.

IV. SSI as Radiometric Quality Index for Deep-Space Observables Troposphere Calibration

In this section, we report the results of the analysis detailed in Section III for each Cassini flyby listed in Table I. The instantaneous *SSI* value, computed as described in Section III-B, is compared with the reference value resulting in a two-state quality index (above or below the threshold) that is used as an ON–OFF indicator to envisage the use of the AMC time series. The *SSI* performance is evaluated through the comparison, pass-by-pass, of the so-derived range rate residuals, in terms of their rms values, with those given by the TSAC calibration. Table II reports the typical parameters used to validate the OD solutions. In particular, M is the mean value of the residuals in mm/s, RMS is the root mean square of the residuals in mm/s, and N is the number of points (residuals) in the pass. In this table, we report the three parameters for both the AMC and TSAC solutions. In each single pass, an M value closer to zero means that there is lesser bias between the observed and the computed deep-space observables. M is expected to be as close as possible to zero to assess the quality of the OD solution.

The use of different path delay calibration time series may result in a different N value in the two solutions from the OD process, and the comparison is meaningful if the N difference is in the order of 1%.

We point out that in 2003, at the beginning of the tour phase of the Cassini mission, the Ka-band translator (KAT) that allows the multifrequency link failed. This is a crucial aspect for the mission and for the radio science experiments, because the solar plasma noise cannot be completely removed. As described in [13] and [14], the tropospheric path delay is the main source of error in the Doppler observables when the plasma noise is completely removed.

For this reason, the advantage to use a more accurate troposphere calibration technique can be less evident due to the uncalibrated plasma noise. In terms of rms, it leads to a smaller difference between the two calibration techniques.

As we can see in Table II, comparing the M and N parameters for each flyby results that the OD solutions are comparable. The M values are close to zero and the N values are mainly the same according to the introduced and expected tolerance.

As far as the rms values are concerned, the analysis on the computed absolute difference between the two values per flyby shows that, among the 17 analyzed cases, the AMC calibrated solutions provides a smaller rms value in 12 cases. In addition, seven cases among those favorable ones give an improvement greater than 25% with a maximum in the order of 50% (the second pass during Titan_T33 flyby). For the cases where the TSAC time series better calibrate the observables, the difference is below 10%, with only one case in the order of 20% (the second pass during Titan_T11). A further inspection indicates that the AMC fails to retrieve the path delay as the spacecraft was tracked under heavy clouds or rainy conditions (as suggested from a retrieved LWC above the 200 μm).

Table II is a snapshot of the use of the two calibration techniques for all available passes regardless of the atmospheric conditions and the indications given by either the AMC flag products or the *SSI* values. The "AMC products" are provided with the automatic algorithms developed by JPL to characterize the sky status with different parameters, thus giving ancillary information about the LOS path. Namely, these are the LWC retrieval and the wind velocity flags as described in Section II-A.

Here, we compare the *SSI* and the AMC products indications for addressing the use of AMC calibration in terms of correlation between the two techniques. As far as *SSI* is concerned, an advantage of using the AMC calibration with respect to the TSAC is foreseen when the instantaneous *SSI* values from the AWVR measurements for a pass are below the *SSI* clear-sky

TABLE II
RANGE RATE RESIDUALS RMS AND MEAN VALUE OBTAINED WITH TSAC AND AMC CALIBRATION

	#	TSAC			AMC		
		M (mm/s)	RMS (mm/s)	N	M (mm/s)	RMS (mm/s)	N
Enceladus_E12	1	9.50E-05	0.004194	271	3.81E-05	0.004288	269
Iapetus	1	3.10E-03	0.111748	132	4.72E-03	0.077673	131
Rhea_4	1	5.32E-04	0.022363	330	4.19E-05	0.020456	328
	2	5.68E-03	0.030391	153	7.16E-03	0.031732	151
	3	−3.32E-04	0.021714	331	4.01E-04	0.019662	331
Saturn_Rev28	1	9.61E-06	0.033716	371	1.50E-04	0.029961	371
Saturn_Rev68	1	1.17E-05	0.026014	245	3.76E-05	0.021044	245
Titan_T11	1	3.19E-04	0.034045	314	7.64E-04	0.022472	313
	2	1.43E-05	0.025494	437	1.44E-03	0.031234	437
	3	2.02E-04	0.024612	385	1.11E-04	0.017001	383
Titan_T22	1	8.52E-05	0.044444	401	2.43E-03	0.024772	399
	2	4.83E-04	0.02274	197	2.73E-03	0.016832	197
Titan_T33	1	1.32E-03	0.037659	453	2.88E-03	0.031581	499
	2	2.65E-04	0.048616	207	1.31E-03	0.024167	207
	3	2.11E-03	0.049268	389	2.70E-03	0.02706	447
Titan_T45	1	2.15E-03	0.067852	504	8.58E-03	0.075971	504
Titan_T68	1	3.41E-03	0.03939	443	4.23E-03	0.040425	443

reference. As far as AMC products, the use of AMC calibration is envisaged when all the flags are zero, the LWC is below 20 m and the wind speed is below 10 m/s.

The results of the analysis are given in Table III as a contingency table. The comparison consists in matching the "AMC products" with the *SSI* trend to analyze the correlation between the two techniques. The first column gives the flyby event. In the second column, "AMC products," two are the possible values: "A" or "T" according to the calibration suggested by the AMC flags, "AMC" or "TSAC," respectively. In the third column, "SSI," the possible labels are "Above," "Below," or "Event" and describe the instantaneous *SSI* time series with respect to the *SSI* reference. The first two terms label the value of the instantaneous *SSI* with respect to the reference one; then, "TSAC" or "AMC" are suggested accordingly. The label "Event" signals cases in which *SSI* correctly detects the sky status as clear sky or in presence of clouds, and, for the longest portion of the time, the instantaneous *SSI* is below the threshold still envisaging the use of the AMC calibration. The fourth column reports the meteorological conditions during the passes in the cases where clouds are present. The column "Preferred Calibration" gives the calibration method that provided the lower rms as listed in Table II. The main result of our analysis is reported in the column "Validation." Here, we use the label: 1) "SSI," if the *SSI* correctly envisaged the most accurate calibration, TSAC or AMC according to the status of the sky; 2) "AMC products," if the correct prevision is done by the AMC flag products; 3) "both" when both techniques agree in the suggested calibration; and 4) "none" if none of them succeed in suggesting the most accurate calibration to be applied.

As expected, in most cases, the two techniques agree, meaning that both the *SSI* and the AMC products choose correctly between the two systems (AMC or TSAC) the one that better calibrates the observables. A deeper look reveals that in two specific cases, Titan_T68 and Enceladus_E12, *SSI* correctly indicates the use of the TSAC with respect to the AMC products. In three other cases, identified as "Event" in the *SSI* column, *SSI* envisaged the use of AMC calibration as the most appropriate technique. Moreover, there are three further cases for which none of the two indicators suggested the use of the AMC calibration, even if its use would have resulted in a better calibration, i.e., a smaller rms value. Nevertheless, especially for the cases within Rhea_4, the difference in the residual rms is minimal probably related to the extremely windy conditions. These cause an increase in the antenna mechanical noise that overwhelms the troposphere error [12]. In the case of the Saturn_Rev68, the relative humidity (RH) time series reported values in the order of 60% (very high for the remote area of the DSS 25) and the CLD flag detected LWC values below 20 μm. In this case, both *SSI* and AMC were above the threshold and the use of AMC was not envisaged, although it was demonstrated that AMC provided a better rms. This case, together with the three "Event" cases successfully calibrated by using AMC, may suggest that AMC could accurately calibrate the

TABLE III
RESIDUALS ESTIMATION: CONTINGENCY TABLE

	AMC products	SSI	Notes and events	Preferred calibration	Validation
Enceladus_E12	A	Above		TSAC	SSI
Iapetus_S33	A	Below		AMC	Both
Rhea_4	T	Above	Cloudy and windy	AMC	none
	T	Above	Cloudy and windy	TSAC	Both
	T	Above	Cloudy and windy	AMC	none
Saturn_Rev28	A	Below		AMC	Both
Saturn_Rev68	T	Above		AMC	none
Titan_T11	T	Event	Clouds	AMC	SSI
	T	Above	Clouds	TSAC	Both
	A	Event	Clouds	AMC	Both
Titan_T22	T	Event	Heavy clouds	AMC	SSI
	T	Event	Heavy clouds	AMC	SSI
Titan_T33	A	Below		AMC	Both
	A	Below		AMC	Both
	A	Below		AMC	Both
Titan_T45	T	Above	Clouds	TSAC	Both
Titan_T68	A	Above		TSAC	SSI

troposphere even in the presence of small amounts of liquid, although in our analysis, only the clear and the nonclear-sky conditions were discriminated. If this is the case, the *SSI* threshold could be modified to include a certain level of liquid water.

With respect to the available CLD flag from the AMC products, the advantage of using the *SSI* is that it allows discriminating radiometric measurements without the need of LWC retrieval algorithms and other instruments measurements rather than AWVR. This aspect can be crucial, in particular, if some of the components are affected by malfunctioning. This specific situation happened in 2011–2012, when the MTP unit of the AMC installed in Goldstone experienced a fault that affected the flag time series. In such a case, the combined use of the AMC products and the *SSI* may give further indication in that sense.

V. CONCLUSION

In this work, the *SSI* criterion was extended to be used with a steerable radiometer, during deep-space tracking, with the purpose of addressing the effectiveness of the AMC-based calibration. Our analysis showed that 1) *SSI* is a useful tool supporting the use of microwave radiometers for the calibration of Doppler observables during deep space tracking experiments, and 2) the improvements (in the form of decrease in the rms values of the Doppler residuals) in the OD process demonstrated the validity of using accurate tropospheric path-delay estimates from AWVR measurements (AMC-based calibration) in clear-sky conditions. The advantages of using *SSI* are manifold.

1) *SSI* approach is suitable for a real-time, automatic, and easy-to-use procedure for employing radiometric data.
2) In deep-space tracking and other applications using MWRs, often concurrent measurements from additional and/or ancillary instruments aid to the screening of the diverse atmospheric conditions. This issue is even more relevant on slant path, when such information is often not available. The *SSI* method relies on radiometric measurements alone to accurately discriminate between atmospheric conditions on the slant path.
3) In the observable calibration procedure, the computation of the *SSI* and its correlation with the "AMC products" helped to promote the use of the AMC calibration during clear-sky conditions. In this case, before processing the deep-space observables in the OD software, *SSI* can also be useful in evaluating the behavior of the AMC time series.
4) Theoretical c_0 and *SSI* values can, in principle, be computed from MWR measurements when RAOBs are not available, showing that the method is fully stand alone.
5) *SSI* can be computed using different pairs of frequencies, sensitive to water vapor and cloud liquid water in the atmosphere, respectively. For instance, frequency channels at 30 or 90 GHz, as found in commercial radiometers, could be used to replace the 31.4-GHz channel. Similar considerations also apply to the 23-GHz channel although this frequency is preferred as it is better suitable for the integrated water vapor estimate.

ACKNOWLEDGMENT

The authors wish to acknowledge the JPL's Radio Science Systems Group for the delivery of the AMC data. Also, they wish to thank Prof. L. Iess, Dr. M. Parisi, Dr. S. Finocchiaro (University La Sapienza, Rome, Italy), and Dr. M. Zannoni (University of Bologna, Bologna, Italy) for the computation of the OD solutions.

REFERENCES

[1] X. Xie, U. Löhnert, S. Kneifel, and S. Crewell, "Snow particle orientation observed by ground-based microwave radiometry," *J. Geophys. Res.*, vol. 117, no. D02206, p. 12, 2012. doi: 10.1029/2011JD016369.

[2] E. F. Campos, R. Ware, P. Joe, and D. Hudak, "Monitoring water phase dynamics in winter clouds," *Atmos. Res.*, vol. 147–148, pp. 86–100, 2014. doi: 10.1016/j.atmosres.2014.03.008.

[3] D. Cimini, M. Nelson, J. Güldner, and R. Ware, "Forecast indices from ground-based microwave radiometer for operational meteorology," *Atmos. Meas. Tech. Discuss.*, vol. 7, pp. 6971–7011, 2014.

[4] C. Mallet and J. Lavergnat, "Beacon calibration with a multifrequency radiometer," *Radio Sci.*, vol. 27, no. 5, pp. 661–680, 1992.

[5] V. Mattioli *et al.*, "Instruments, data and techniques for the assessment of the atmospheric noise emission in Satcom ground stations," in *Proc. 6th Eur. Conf. Antennas Propag. (EUCAP'12)*, Prague, Czech Republic, Mar. 26–30, 2012, pp. 76–80.

[6] S. J. Keihm and K. A. Marsh, "Advanced algorithm and system development for Cassini radio science tropospheric calibration," Jet Propulsion Lab., Pasadena, CA, USA, The Telecommunications and Data Acquisition Progress Report 42-127, 1996, pp. 1–20.

[7] K. Ebell, E. Orlandi, A. Hünerbein, U. Löhnert, and S. Crewell, "Combining ground and satellite based measurements in the atmospheric state retrieval: Assessment of the information content," *J. Geophys. Res.*, vol. 18, pp. 6940–6956, 2013.

[8] M. P. Cadeddu, J. C. Liljegren, and D. D. Turner, "The atmospheric radiation measurement (ARM) program network of microwave radiometers: Instrumentation, data, and retrievals," *Atmos. Meas. Tech.*, vol. 6, no. 9, pp. 2359–2372, 2013. doi: 10.5194/amt-6-2359-2013.

[9] D. D. Turner, M. P. Cadeddu, U. Löhnert, S. Crewell, and A. M. Vogelmann, "Modifications to the water vapor continuum in the microwave suggested by ground-based 150-GHz observations," *IEEE Trans. Geosci. Remote Sens.*, vol. 47, no. 10, pp. 3326–3337, Oct. 2009.

[10] B. Bertotti, L. Iess, and P. Tortora, "A test of general relativity using radio links with the Cassini spacecraft," *Nature*, vol. 425, pp. 374–376, Sep. 2003.

[11] V. Mattioli, E. R. Westwater, S. Gutman, and V. Morris, "Forward model studies of water vapor using scanning microwave radiometers, global positioning system and radiosondes during the cloudiness intercomparison experiment," *IEEE Trans. Geosci. Remote Sens.*, vol. 43, no. 5, pp. 1012–1021, May 2005.

[12] D. D. Turner, S. A. Clough, J. C. Liljegren, E. E. Clothiaux, K. E. Cady-Pereira, and K. L. Gaustad, "Retrieving liquid water path and precipitable water vapor from the Atmospheric Radiation Measurement (ARM) microwave radiometers," *IEEE Trans. Geosci. Remote Sens.*, vol. 45, no. 11, pp. 3680–3690, Nov. 2007.

[13] L. Iess, M. Di Benedetto, N. James, M. Mercolino, L. Simone, and P. Tortora, "Astra: Interdisciplinary study on enhancement of the end-to-end accuracy for spacecraft tracking techniques," *Acta Astronaut.*, vol. 94, no. 2, pp. 699–707, Feb. 2014. ISSN 0094-5765 [Online]. Available: http://dx.doi.org/10.1016/j.actaastro.2013.06.011.

[14] P. Tortora *et al.*, "Instruments, data and techniques for the assessment of tropospheric noise in deep space tracking," in *Proc. 6th Eur. Conf. Antennas Propag. (EUCAP'12)*, Prague, Czech Republic, Mar. 26–30, 2012, pp. 106–110.

[15] P. Tortora, L. Iess, J. J. Bordi, J. E. Ekelund, and D. C. Roth, "Precise Cassini navigation during solar conjunctions through multifrequency plasma calibrations," *J. Guid. Control Dyn.*, vol. 27, no. 2, pp. 251–257, 2004.

[16] Y.E. Bar-Sever *et al.*, "Atmospheric media calibration for the deep space network," *Proc. IEEE*, vol. 95, no. 11, pp. 2180–2192, Nov. 2007. doi: 10.1109/JPROC.2007.905181.

[17] A. B. Tanner and A. L. Riley, "Design and performance of a high-stability water vapor radiometer," *Radio Sci.*, vol. 38, no. 3, p. 8050, 2003. doi: 10.1029/2002RS002673.

[18] A.V. Bosisio, E. Fionda, P. Basili, G. Carlesimo, and A. Martellucci, "Identification of rainy periods from ground-based microwave radiometry," *Eur. J. Remote Sens.*, vol. 45, pp. 41–50, 2012. doi: 10.5721/EuJRS20124505.

[19] L. Iess *et al.*, "Tides of Titan," *Science*, vol. 337, p. 457, 2012.

[20] L. Iess *et al.*, "The gravity field and interior structure of enceladus," *Science*, vol. 344, no. 6179, pp. 78–80, 2004. doi: 10.1126/science.1250551.

[21] N. D. Panagiotacoupulos, J. W. Zielenbach, and R. W. Duesing, *An Introduction to JPL's Orbit Determination Program*. Pasadena, CA, USA: Jet Propulsion Lab., National Aeronautics and Space Administration, 1974.

[22] T. D. Moyer, *Formulation for Observed and Computed Values of Deep Space Network Data Types for Navigation*. Hoboken, NJ, USA: Wiley, 2003.

[23] F. H. Webb and J. F. Zumberge, *An Introduction to GIPSY/ OASIS-II*. Pasadena, CA, USA: Jet Propulsion Lab., JPL Publication D-11088, 1997.

[24] G. M. Resch, "Inversion algorithms for water vapor radiometers operating at 20.7 and 31.4 GHz," TDA Prog. Rep. 42-76, Oct. 1983, pp. 12–26.

[25] S. J. Kehim and K. A. Marsh, "New model-based Bayesian inversion algorithm for the retrieval of wet troposphere path delay from radiometric measurements," *Radio Sci.*, vol. 33, no. 2, pp. 411–419, 1998.

[26] A.V. Bosisio, P. Ciotti, E. Fionda, and A. Martellucci, "A sky status indicator to detect rain-affected atmospheric thermal emissions observed at ground," *IEEE Trans. Geosci. Remote Sens*, vol. 51, no. 9, pp. 4643–4649, Sep. 2013.

[27] V. Mattioli, A. Graziani, P. Tortora, A. V. Bosisio, and L. Castanet, "Analysis and improvements of methodologies for discriminating atmospheric conditions from radiometric brightness temperatures," in *Proc. 7th Eur. Conf. Antennas Propag. (EuCAP)*, Gothenburg, Sweden, Apr. 8–12, 2013, pp. 1392–1396.

[28] B. E. Schwartz and M. Govett, "A hydrostatically consistent North American Radiosonde Data Base at the forecast Systems Laboratory, 1946-present," NOAA Technical Memorandum ERL FSL-4, NTIS PB 112225, 1992.

[29] V. Mattioli *et al.*, "Analysis of radiosonde and ground-based remotely sensed PWV data from the 2004 North Slope of Alaska Arctic Winter Radiometric Experiment," *J. Atmos. Ocean. Tech.*, vol. 24, no. 3, pp. 415–431, Mar. 2007. doi: 10.1175/JTECH1982.1.

[30] J. A. Schroeder and E. R. Westwater, "Users' guide to WPL microwave radiative transfer software," NOAA/Environmental Research Lab., Boulder, CO, USA, NOAA Tech. Rep. ERL-219 WPL-213, 1991, 84 pp.

[31] P. W. Rosenkranz, "Water vapor microwave continuum absorption: A comparison of measurements and models," *Radio Sci.*, vol. 33, no. 4, pp. 919–928, 1998.

[32] P. W. Rosenkranz, "Correction to water vapor microwave continuum absorption: A comparison of measurements and models," *Radio Sci.*, vol. 34, no. 4, p. 1025, 1999.

[33] V. Mattioli, P. Basili, S. Bonafoni, P. Ciotti, and E. R. Westwater, "Analysis and improvements of cloud models for propagation studies," *Radio Sci.*, vol. 44, p. RS2005, Mar. 2009. doi: 10.1029/2008RS003876.

[34] Y. Han and E. R. Westwater, "Analysis and improvement of tipping calibration for ground-based microwave radiometers," *IEEE Trans. Geosci. Remote Sens.*, vol. 38, no. 3, pp. 1260–1276, May 2000.

Ada Vittoria Bosisio (M'00) received the M.S. degree in electronic engineering and the Ph.D. degree in applied electromagnetism from the Politecnico di Milano, Milano, Italy, in 1991 and 1995, respectively.

During her Doctorate degree, she was involved in the Olympus and Italsat propagation experiments for the aspects related to propagation-oriented radiometry (Ka band). From 1995 to 1997, she joined as a Research Associate with the CETP/CNRS Laboratory, Vélizy, France, where she has been active in measurements and analysis of forest attenuation and scattering at 2 and 6 GHz. From 1997 to 1998, she joined CNET/France Telecom, Issy Les Mx., France, as *Ingenieur de Recherche*, working on radio wave effects induced by GSM on the environment and on individuals. From 1999 to 2001, she was with the Propagation Group, Politecnico, Milano, Italy, as a Research Associate working on satellite links at low elevation angle in K- and W-band and on propagation of TV broadcast and digital radio links over mountains through ray techniques. Since 2001, she has beena Researcher with Italian National Research Council, IEIIT Institute, Milano, Italy, working in remote sensing applications related to atmospheric science and tropospheric propagation. Her research interests include channel modeling in indoor environments affected by dense multipath fading effects for localization and tracking purposes, interaction mechanisms between signal and complex media.

Alberto Graziani received the B.Sc. and M.Sc. degrees in aerospace engineering, and the Ph.D. degree in industrial engineering from the University of Bologna, Bologna, Italy, in 2003, 2006, and 2010, respectively.

Since 2013, he has been a Postdoctoral Researcher with the Université Catholique de Louvain, Louvain-la-Neuve, Belgium. His research interests include characterization of the troposphere as transmission media for space missions links: deep space and Earth orbit missions.

Dr. Graziani was a member of the COST Action IC0802, from 2009 to 2012.

Vinia Mattioli received the M.S. degree in electronic engineering and the Ph.D. degree in information engineering from the University of Perugia, Perugia, Italy, in 2001 and 2005, respectively.

Since 2006, she is an Affiliate of the Center for Environmental Technology (CET), Department of Electrical and Computer Engineering, University of Colorado, Boulder, CO, USA. Between 2005 and 2013, she was a Postdoctoral Research Associate with the Department of Electronic and Information Engineering, University of Perugia, where she also served as a Teaching Assistant for undergraduate and graduate courses in remote sensing and electromagnetic field theory. From 2007 to 2009, she served as an Adjunct Professor with the University of Perugia at Orvieto, Orvieto, Italy. Between 2012 and 2013, she was a Visiting Researcher with the Electromagnetics and Radar Department, Onera, Toulouse, France, as a Microwave Radiometer Expert for radio propagation applications. She was a part of the Management Committee in the COST280 international project on propagation and telecommunications. Since 2013, she has been working with EUMETSAT on the development of calibration algorithms for the MWI and ICI instruments that will be on board of the Eumetsat Polar System–Second Generation. Her research interests include radiometer calibration techniques, passive ground-based and satellite-based microwave atmospheric remote sensing, physical and statistical modeling for radio propagation applications, microwave radiative transfer models, and GPS applied to remote sensing.

Paolo Tortora (M'99) received the Laurea degree in aeronautical engineering and the Ph.D. degree in aerospace engineering from the University of Rome "la Sapienza," Rome, Italy, in 1997 and 2001, respectively.

Since 2002, he has been associated with the University of Bologna, Bologna, Italy, where he leads research activities ranging from small satellite missions and applications to radio science experiments on deep space probes and interplanetary navigation. Currently, he is an Associate Professor in Astronautics and Space Systems, leads the "Microsatellites and Micro Space Systems" and "Radio Science and Planetary Exploration" Laboratories and, since 2012, chairs the B.Sc. and M.Sc. degrees Programs in Aerospace Engineering.

Dr. Tortora is an Associate Editor of the following journals: *Advances in Aerospace Science and Technology*, the *International Journal of Aerospace Engineering*, the *International Journal of Aeronautical Science and Aerospace Research*, the *Journal of Small Satellites,* and the *Online Journal Positioning*. He is a member of the AIAA and ION.